Stochastic Environmental Research and Risk Assessment (2022) 36:1597–1614
https://doi.org/10.1007/s00477-021-02073-2

ORIGINAL PAPER

Investigating seasonal drought severity-area-frequency (SAF) curve over Indian region: incorporating GCM and scenario uncertainties

Subhadarsini Das[1] · Jew Das[1] · N. V. Umamahesh[1]

Accepted: 5 August 2021 / Published online: 12 August 2021

Abstract
Understanding the devastating nature of drought, this work has assessed the variability in the Severity-Area-Frequency (SAF) curve using Standardised Precipitation Evapotranspiration Index (SPEI) as meteorological drought indicator over Maharashtra, India. The future meteorological outputs from 19 Global Circulation Models (GCMs) of the NASA Earth Exchange Global Daily Downscaled Projections (NEX-GDDP) under two Representative Concentration Pathway (RCP) 4.5 and 8.5 are used. The SAF curves are developed for five different seasons namely pre-monsoon, monsoon, post-monsoon, Kharif and Rabi. The uncertainty associated with GCMs and scenarios is assessed using possibility theory. The results reveal that the precipitation magnitude is expected to increase in pre-monsoon, monsoon, and Kharif seasons over most of the areas in Maharashtra. However, the temperature is likely to increase during all the seasons in future. The frequency of extreme drought condition during post-monsoon, pre-monsoon, and Rabi seasons shows an increment as compared to historical period. The Rabi season drought is noticed to be most pronounced and likely to affect significant portions of Maharashtra during all return periods. The SAF curve reveals that, in most of the cases, the percentage of drought affected area is expected to increase for high magnitude of severity.

Keywords SAF curve · Seasonal drought · SPEI · NEX-GDDP · Uncertainty analysis

1 Introduction

The demand of water has increased profoundly due to population growth and expansion of agricultural and industrial sectors. On the other hand, the dual pressure of climate change and its spatio-temporal variability has contributed to water scarcity. The recurrent water scarcity is likely to influence the economic and human development, and natural hazards with increased severity can aggravate the situation (Amarasinghe et al. 2020). The modulation in the various extreme weather events, as a result of changing climatic conditions, influences the frequency and severity of different natural hazards (e.g., drought, flood, among others). Drought, as most devastating and costliest natural hazard, has adverse consequences on ecological system and many economic sectors (Tallaksen and Van Lanen 2004; Sheffield and Wood 2012). In recent past, due to the anthropogenic alterations and changes in the climatic parameters, severe drought events have increased significantly across the globe (Trenberth et al. 2014; AghaKouchak et al. 2015; Van Loon et al. 2016; Das et al. 2021a). In addition, due to the lack of precise definition of drought (Lloyd-Hughes 2014; Das et al. 2021b), it is cumbersome to identify the initiation and termination of drought events making it more challenging to deal with. Therefore, it is inevitable for water managers and decision makers to understand the impacts of drought associated with different severity levels in order to take suitable adaptive measures (Svoboda et al. 2002).

Focussing on the stochastic nature of water demand in different regions as a consequence (directly or indirectly) of variability in the hydro-climatic variables and other anthropogenic activities, various drought indices have been developed. For instance, based on deficit in precipitation, Standardised Precipitation Index (SPI) is widely used to examine the meteorological drought. However, Standardised Precipitation Evapotranspiration Index (SPEI) (Vicente-Serrano et al. 2010) determines the drought events more reliably as it incorporates both precipitation and

✉ Jew Das
jewdas05@gmail.com

[1] Department of Civil Engineering, National Institute of Technology Warangal, Warangal, India

potential evapotranspiration in its calculation. Moreover, as the cumulative effect of moisture deficit over different time periods causes drought events, the indices should be analysed for various time scale to get a clear picture of drought. Likewise, future drought forecasting for short- and long-time scales provides required information about climatic conditions to farmers (Bisht et al. 2019; Das et al. 2021a) and policy makers, respectively.

At least once every 3 years, India is negatively impacted by drought conditions and considered amongst the most vulnerable and drought-prone countries in the world (Mishra and Singh 2010; Mishra et al. 2019). In recent times, prolonged and widespread drought condition with increased frequency has been observed over India (Lester and Gurenko 2003; Mishra and Singh 2010; Sharma and Goyal 2020). Hence, it is well understood that drought is likely to affect the overall economy of the country under the climate sensitive economic sectors in India (Udmale et al. 2014; Shah and Mishra 2020). For instance, it was reported that widespread drought is likely to impact the Indian economy by $100 billion (ASSOCHAM Report 2016). Since the country is largely reliant on the water resources (mostly in the form of precipitation), shift in the drought pattern as a result of climate change may have extensive impacts on population and economy. With this understanding, projection of future drought at short- and long-term scales enable to formulate improved management practices i.e., water harvesting schemes, land management practices, drought resistant technologies, groundwater management practices, crop and livestock insurance etc. in order to tackle with the adverse consequences of future drought events.

General Circulation Models (GCMs) are considered as credible tools in simulating long-term climate projections under different climate change scenarios (Mishra and Singh 2009; Shivam and Sarma 2017; Khan et al. 2018; Her et al. 2019). In general, GCMs are modelled mathematically by considering the physical processes across ocean, land and atmosphere (Sachindra et al. 2013). Therefore, the essential hydro-climatic variables simulated by GCMs can be used for drought predictions. In past studies, several GCMs under the Coupled Model Intercomparison Project 3 (CMIP3) and 5 (CMIP5) were used to examine different types of drought events across the world (Mishra et al. 2014; Ahmadalipour et al. 2017; Spinoni et al. 2018, 2019). In order to project drought at regional scale, the outputs from GCMs should be downscaled from coarser spatial resolution to finer resolution. Presently, outcomes from the GCMs are readily available at finer spatial resolution using different downscaling techniques and can be obtained from but are not limited to Coordinated Regional Climate Downscaling experiment (CORDEX) and NASA Earth Exchange Global Daily Downscaled Climate Projections (NEX-GDDP).

However, initial parametrisation, formulation, model structure, and input data used for development of GCMs can impose uncertainty in the final climate projections (Mishra et al. 2014; Khan et al. 2020). Likewise, the uncertainty associated with the future climatic scenarios can be attributed to incomplete understanding and unpredictability about the foreseen climate (New and Hulme 2000). Thus, in order to devise sustainable planning and decision- making, the practitioners should consider the uncertainty for future climate scenarios (Höllermann and Evers 2017). With this understanding, previous studies used different techniques but are not limited to sensitivity analysis (Mearns et al. 1996), Monte Carlo simulation (Shackley et al. 1998), reliability ensemble averaging (Giorgi and Mearns 2003), imprecise probability (Ghosh and Mujumdar 2009), Fuzzy uncertainty analysis (Najafi and Hessami Kermani 2017), Bayesian analysis (Das and Umamahesh 2018). In the present study, in order to quantify the GCMs and scenario uncertainty, possibility theory is used. The possibility theory assigns the possibility distribution based on the ability of GCMs and emission scenarios to model the recent past under climate forcing (Das et al. 2020b). The possibility approach is computationally inexpensive, straightforward, and useful in addressing partially inconsistent knowledge and linguistic information based on intuitions (Mujumdar and Ghosh 2008).

The past records of different drought indices show increased aridity over many land areas since 1950 (Dai 2011a, b). Moreover, the drought risk is likely to increase in the twenty-first century as suggested by different studies (Rind et al. 1990; Burke and Brown 2008; Aadhar and Mishra 2018; Poonia et al. 2021a, b; Spinoni et al. 2018, 2020). Thus, it is necessary to incorporate different drought characteristics in order to evaluate the changes in drought events properly. For example, Severity-Area-Frequency (SAF) relationship curve can be used for providing quantitative information about drought through characterising various attributes of drought like return period, areal extent and severity (Henriques and Santos 1999). Therefore, SAF relationship has been used to understand the nature of spatio-temporal characteristics of drought at regional scale. For example, Reddy and Ganguli (2013) used SAF analysis to understand the drought characteristics over western Rajasthan (India); recurrence pattern of meteorological drought severity was carried out using SAF curve in the upper Blue Nile river region (Khadr 2017); SAF was used to perform the regional analysis of drought in Lake Urmia basin, Iran (Amirataee et al. 2018) and Heihe River basin (China) (Li et al. 2020). However, most of the SAF analysis studies are executed for the historical

time period. Thus, the present study focuses on the possible future variability in the seasonal SAF curve ascertaining the uncertainties associated with GCMs and scenarios.

The purpose of this study is to develop seasonal (pre-monsoon, monsoon, post-monsoon, Rabi, and Kharif) SAF curve under meteorological drought condition over the study area. In addition, the study aims to make the future projection of the seasonal SAF curve ascertaining the uncertainty associated with GCMs and scenarios. The SPEI drought index is used as an indicator of meteorological drought. In order to project for the future time period, nineteen different GCMs under two different Representative Concentration Pathways (RCPs) 4.5 and 8.5 are chosen. Maharashtra, as a drought-prone state is selected to perform the analysis. To the best of the authors' knowledge, no such multifaceted investigation of drought has been carried out over Maharashtra. It is expected that the outcomes from the present study can be helpful in drought risk mitigation planning over the study area.

2 Study area and data source

2.1 Study area

Maharashtra, the drought-prone state in India is considered as a physical area for this study. This state incorporates about 24% of total drought affected area in India according to Maharashtra state Agriculture Portal. The state has experienced 11 out of 26 droughts during 1901–1998 (Gore and Ray 2002) with a monotonically spatially increasing trend of drought during 1951–2010 (Sharma and Mujumdar 2017). Agriculture has been the backbone of the state as 82% of the rural population depend on it. Agriculture sustainability mainly depends on the precipitation over the state and the variability in the meteorological variables are likely to change under climate variability (Kelkar et al. 2020). Therefore, focussing on the above descriptions, Maharashtra has been selected for future seasonal drought analysis which would be helpful for farmers and policy-makers for better dealing with future drought events with sustainable drought management plan.

The areal extent of Maharashtra is about 307,713 km^2 and considered as third largest state in the country. The state consisting of six divisions, namely Konkan, Nashik, Pune, Aurangabad, Amaravati, Nagpur falls between 72° 0.64′ N and 80° 0.90′ N longitudes and 15° 0.61′ E to 22° 0.03′ E latitudes (Fig. 1). The mean annual precipitation is recorded as 1133 mm with significant spatial variability. Similarly, the maximum and minimum temperature varies in the range of 37 °C to 46 °C and 3 °C to 12 °C, respectively. To analyse the seasonal drought variability, pre-monsoon (March to May), monsoon (June to September), post-monsoon (October to December), Rabi (October to March) and Kharif (July to October) seasons are considered.

2.2 Data sources

2.2.1 Observed datasets

The daily meteorological observations such as precipitation, maximum and minimum temperature are collected for 68 years (1951–2018) from India Meteorological Department (IMD), Pune. The original gridded precipitation datasets with spatial resolution (0.25° × 0.25°) have been developed using 6955 rain gauge stations (Pai et al. 2014). Similarly, 395 quality controlled temperature stations (Srivastava et al. 2009) have been used for preparing temperature datasets with 1° × 1° spatial resolution. These high-resolution datasets help in capturing the spatial distribution of rainfall and temperature with more accuracy (Pai et al. 2014). Considering the accuracy level, many researchers (Sharma and Mujumdar 2017; Jha et al. 2019; Das et al. 2020a) have successfully used these high-resolution datasets in their studies.

2.2.2 GCM projected datasets

The NASA Earth Exchange Global Daily Downscaled Projections have temperature (maximum and minimum) and precipitation data for the period from 1950 through 2100; where data from 1950 through 2005 and from 2006 to 2100 are considered for the retrospective run and prospective run, respectively. These meteorological datasets are downscaled under two climate scenarios i.e. RCP 4.5 and RCP 8.5 derived from 21 GCMs conducted under CMIP5. Bias-Correction-Spatial Disaggregation (BCSD) method (Thrasher et al. 2013) is used for bias correcting daily temperature and precipitation data. The datasets are available with high spatial resolution of 0.25° × 0.25° and can be downloaded from (ftp://cccr.tropmet.res.in/FTPServer/NEX-INDOUS_Data/). Out of 21 GCMs, 19 GCMs are considered in this study because of unavailability of complete datasets in two GCMs. Specifically, NEX-GDDP datasets help project climate change patterns at local and regional scale. Therefore, many researchers (Sahany et al. 2019; Singh et al. 2019; Jain et al. 2019) have successfully evaluated future climate impacts over different parts of the world using NEX-GDDP datasets. The details of the GCMs and their respective institutions are presented in Table 1.

2.2.3 Spatial resolution and time period used

In order to maintain a common grid resolution, each meteorological dataset is re-gridded to 0.5° × 0.5° using

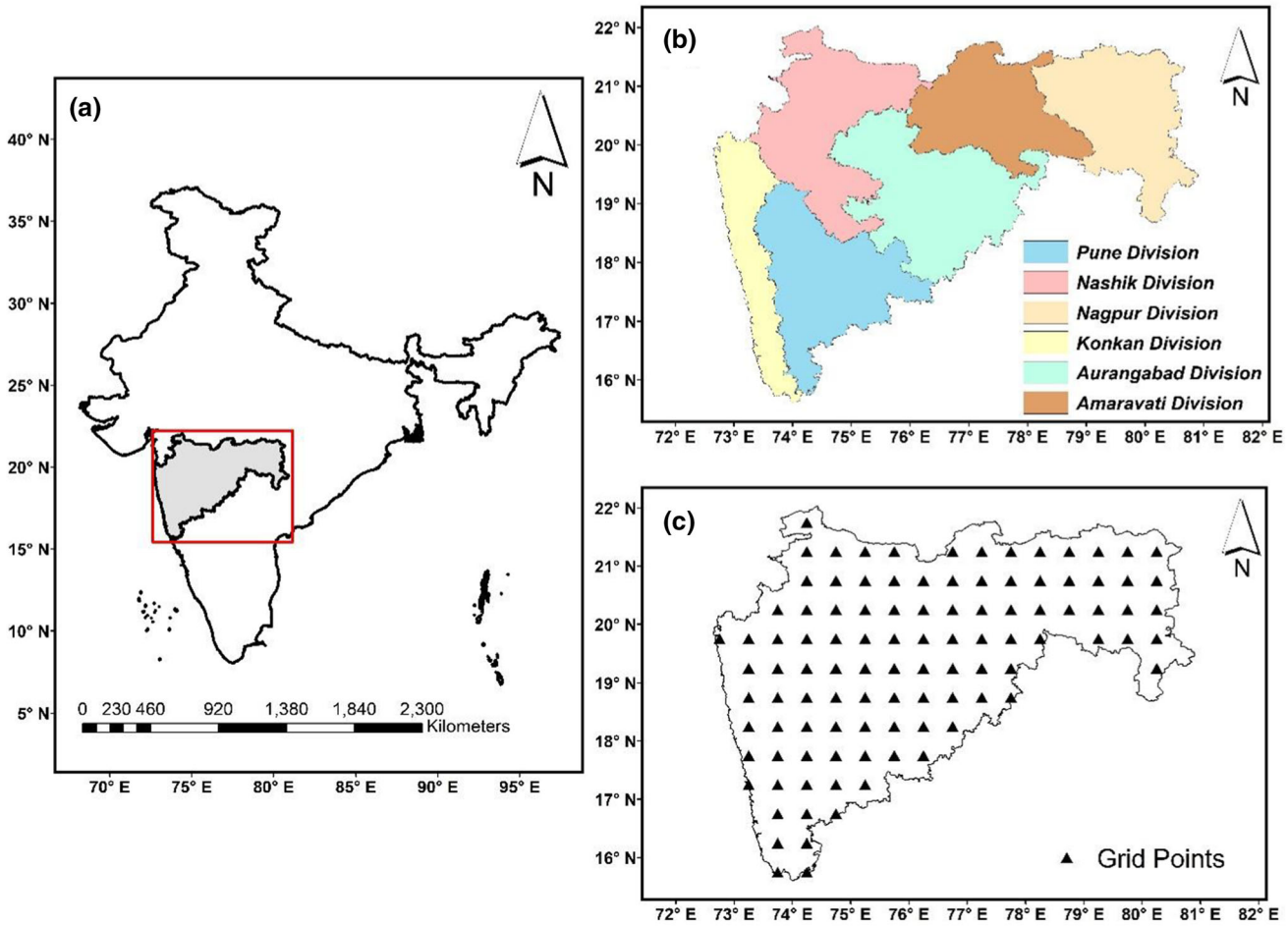

Fig. 1 Details of the study area. **a** Maharashtra superimposed over India Map, **b** Different division across Maharashtra, **c** Grid points over the study area

the bilinear interpolation technique which performs comparatively better among other interpolation techniques such as nearest neighbour, bicubic (Peng et al. 2019). For more detailed information about the bilinear interpolation, interested readers are advised to follow Fischer et al. (2014). According to 0.5° × 0.5° spatial resolution, there are total of 103 grid points covering the study area (Fig. 1c). It is worth mentioning that, the NEX-GDDP data sets has already been bias-corrected using global climate data prepared by the Terrestrial Hydrology Research Group at Princeton University (Sheffield et al. 2006). However, at regional scale, it further needs bias-correction using the datasets available for the region as the number of observation gauges over the area may be more as compared to the historical datasets used to correct initial bias in NEX-GDDP data (Chen et al. 2020). In this sense, time period from 1951 to 2005 is considered as baseline period to bias correct the global climate data (both for historical and future projections). In order to compare the future meteorological drought condition, the future period is segregated in to three equal lengths of 26 years, i.e., 2022–2047 (T1), 2048–2073 (T2), and 2074–2099 (T3). The recent past from 1993 to 2018 (T0) is considered as historical period.

3 Methodology

The overall procedure of this study is described in three parts. The first part checks the correctness of meteorological datasets from 19 NEX-GDDP models by comparing them with observed IMD datasets during baseline period. Next, the bias correction is carried out to reduce biases both in historical and future projection datasets of 19 GCMs. In the second part, SPEI drought indicator has been computed at 3 different time scales (3-, 4-, 6-months) for T0, T1, T2, and T3 periods. The analysis of three different time scales helps to evaluate the changes in seasonal drought severity during future time series as compared to recent past years. In the third part, possibility theory is utilised to ascertain the GCM and scenario uncertainties at

Table 1 List of the GCMs with their respective institution used for the present study

Sl. No	Model	Institution
1	ACCESS1-0 (M1)	Commonwealth Scientific and Industrial Research Organization and Bureau of Meteorology, Australia
2	BCC-CSM1-1 (M2)	Beijing Climate Center, China
3	CanESM2 (M3)	Canadian Centre for Climate Modelling and Analysis, Canada
4	CCSM4 (M4)	National Center for Atmospheric Research, America
5	CESM1-BGC (M5)	National Center for Atmospheric Research, America
6	CNRM-CM5 (M6)	Centre National de Recherches Meteorologiques, Centre Europeen de Recherche et Formation Avancees en Calcul Scientifique, France
7	CSIRO-Mk3-6-0 (M7)	Commonwealth Scientific and Industrial Research Organization/Queensland Climate Change Centre of Excellence, Australia
8	GFDL-CM3 (M8)	Geophysical Fluid Dynamics Laboratory, America
9	GFDL-ESM2G (M9)	Geophysical Fluid Dynamics Laboratory, America
10	GFDL-ESM2M (M10)	Geophysical Fluid Dynamics Laboratory, America
11	INMCM4 (M11)	Institute of Numerical Calculation, Russia
12	IPSL-CM5A-LR (M12)	Institut Pierre-Simon Laplace, France
13	IPSL-CM5A-MR (M13)	Institut Pierre-Simon Laplace, France
14	MIROC-ESM (M14)	Atmosphere and Ocean Research Institute, Japan
15	MIROC-ESM-CHEM (M15)	Atmosphere and Ocean Research Institute, Japan
16	MPI-ESM-LR (M16)	Max Planck Institute for Meteorology, Germany
17	MPI-ESM-MR (M17)	Max Planck Institute for Meteorology, Germany
18	MRI-CGCM3 (M18)	Max Planck Institute for Meteorology, Germany
19	NorESM1-M (M19)	Norway Consumer Council, Norway

each grid point. Lastly, SAF curve curves are estimated for each season, which reveals the percentage of drought affected area associated with specific magnitude of severity for different return periods. The complete methodology is presented in the form of a graphical flow chart (Fig. 2).

3.1 Bias-correction of GCM datasets

The errors in GCMs comprise of unsystematic and systematic components (Teutschbein and Seibert 2013). The unsystematic model errors occur due to the chaotic nature of climate system and their dynamic feedback processes (Christensen et al. 2001). These random errors causes discrepancy between the GCM and observed datasets at time scales ranging from daily to annual (Eden et al. 2012). On this account, different bias-correction techniques are proposed to improve the model outputs from GCMs. In general, these bias- correction techniques are grouped into four different categories namely linear (Lenderink et al. 2007), non-linear (Leander and Buishand 2007), distribution based quantile mapping (Piani et al. 2010), distribution free quantile mapping (Ashfaq et al. 2010). Among all techniques, distribution free quantile mapping method is proved of having the best skill in correcting bias (Lafon et al. 2013). Therefore, in this study, non-parametric quantile mapping is used for bias correction. Here, it is assumed that both internal error in climate models (Hewitson et al. 2014) and scale relationship follows a stationary condition for future projections. Fundamentally, it means that the correction factor estimated during the baseline period is valid for the future period. The bias correction has been performed at each grid point considering 1951–2005 as baseline period. Then the correction factor obtained during 1951–2005 is used for correcting the bias during future periods under RCP4.5 and RCP8.5 scenarios for T1, T2, and T3 timeframes. The Eq. 1 represents the formula used in quantile mapping bias correction technique.

$$V_o = F_o^{-1}(F_m(V_m)) \quad (1)$$

where V_o and V_m represent observed and modelled data, respectively. F_m and F_o^{-1} are the cumulative distribution function (CDF) of V_m and the inverse CDF (transfer function) of V_o, respectively. The detailed methodology is

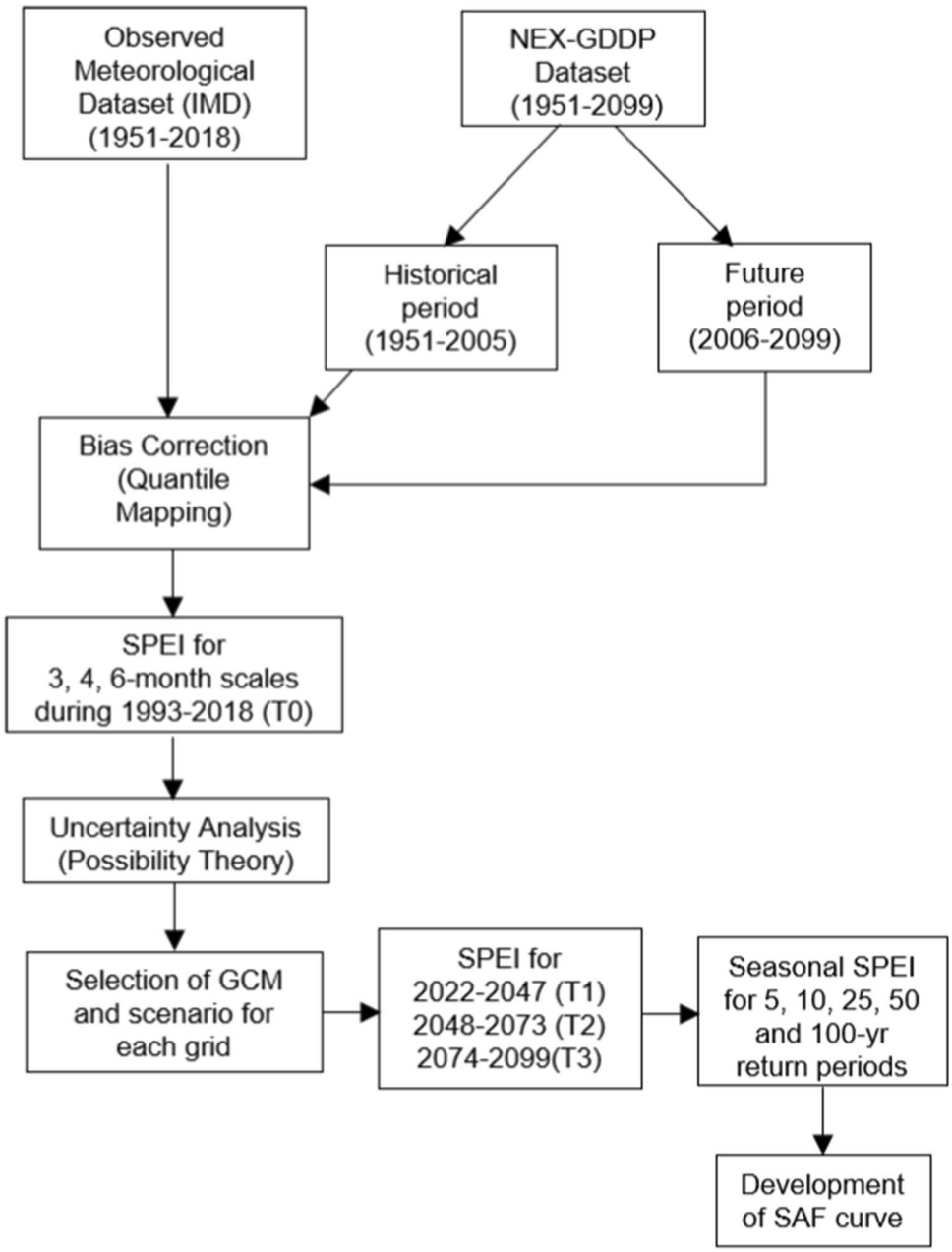

Fig. 2 Flow chart of the proposed study

clearly explained by Gudmundsson et al. (2012). Moreover, the bias-correction is performed using 'qmap' package in R developed by Gudmundsson (2016) and can be downloaded from https://cran.r-project.org/web/packages/qmap/index.html.

3.2 Drought indicator: SPEI

In this study, SPEI drought indicator is selected to determine the influence of combined effect of precipitation and temperature on seasonal drought events. The daily bias-corrected datasets are converted to monthly scale in order to compute the seasonal SPEI. This conversion is done for both IMD datasets and NEX-GDDP datasets (for both historical period and future projections).

In present climate change scenario, due to the growing impacts of global warming, temperature plays a crucial role in the occurrence of drought events. Moreover, it has significant impact on hydrological water balance by controlling meteorological variables like evaporation and precipitation (Dai et al. 2018). In the context of drought analysis, precipitation covers the supply side of the water balance. However, the demand side is represented by PET (evaporative demand) which is a function of temperature, wind speed, humidity, and solar radiation (Kew et al. 2019). Therefore, with increase in temperature, the demand

side of water balance is likely to increase and will aggravate the drought condition. Therefore, the influence of PET should not be neglected in drought analysis (Lin et al. 2020).

Hence, considering the influence of temperature, Vicente-Serrano et al. (2010) developed SPEI as meteorological drought indicator, which takes into account both precipitation and Potential Evapotranspiration (PET). However, the estimation of PET is a challenging task (Milly and Dunne 2016) as the selected methodology in the computation of PET can have impacts on SPEI in some particular regions of the world (Beguería et al. 2014). In general, PET is computed by Penman–Monteith's (Allen et al. 1994) method, Thornthwaite (Thornthwaite 1948) method, and Hargreaves (Hargreaves 1994) method. Among these methods, Penman–Monteith's method is the most widely accepted method to obtain more realistic estimation of PET in the case of drought studies (Trenberth et al. 2014; Zhao and Dai 2017). The meteorological variables like relative humidity, wind speed, cloud cover, sunshine hour along with precipitation and temperature are considered in Penman–Monteith's method. However, in the present study, these meteorological variables except precipitation and temperature are not available in NEX-GDDP experiment for future climate change scenarios. Therefore, Hargreaves method which is proven to be superior than Thornthwaite method (Bandyopadhyay et al. 2012; Aadhar and Mishra 2020) is used in this study. The PET is computed using the "SPEI" package (Begueria et al. 2017) in R and can be downloaded from https://cran.r-project.org/web/packages/SPEI/index.html. Then, 'SCI' package is used for the calculation of SPEI at three different time scales i.e., 3, 4, 6-months. Unlike SPI, SPEI uses monthly water balance (difference between precipitation and PET) instead of monthly precipitation. Additionally, log-logistic distribution (Vicente-Serrano et al. 2010) is adopted as a suitable distribution for SPEI calculation.

The computation of SPEI is initially done for historical period (1951–2005) and then the transformations obtained during historical period are further used to compute SPEI for T0, T1, T2, and T3 time periods. The calculation is carried out at each grid point and each GCM under RCP4.5 and 8.5. The classification of different drought types based on the SPEI value is listed in Table 2.

Table 2 Drought classifications and their range for SPI and SPEI

Classification	Range	Category
Extreme wet	≥ 2.00	EW
Severe wet	1.99 to 1.50	SW
Moderate wet	1.49 to 1.00	MW
Near normal	0.99 to − 0.99	NN
Moderate drought	− 1.00 to − 1.49	MD
Severe drought	− 1.50 to − 1.99	SD
Extreme drought	$\leq$ − 2.00	ED

3.3 Possibility theory for uncertainty analysis

In order to facilitate the risk-based studies on future hydrologic extremes, modelling of GCM and scenario uncertainty plays an important role. In the present climate change scenario, it is relevant to evaluate the usefulness of GCMs in modelling climate change impact and to analyse the ability of scenario to represent the present situation. In this sense, possibility distribution is used to analyse the GCM and scenario uncertainties based on the performance in capturing the climate change signals during the recent past. Zadeh (1999) proposed the possibility theory to address inconsistent knowledge and incomplete information (Dubois 2006). In the present study, the possibility theory is based on the ability of GCM and scenario to simulate the SPEI value at 3-, 4-, and 6-month scales during recent past i.e., T0. Being a measure of how well a GCM with a particular scenario predicts the SPEI values during T0, the Nash–Sutcliffe Efficiency (NSE) is used which provides a measure of possibility value. Unlike the probability, possibility is primarily ordinal and is not associated with frequency of experiments (Mujumdar and Ghosh 2008). The possibility theory postulates that if a variable X in the universe Ω is not possible to estimate precisely, then the possibility that X can take the value x can be expressed mathematically as (Spott 1999)

$$\Pi_X(x) : \Omega \rightarrow [0, 1] \tag{2}$$

where $\Pi_X(x) = 1$ ($\Pi_X(x) = 0$) suggests that X = x is possible (impossible) without any restriction. The property of possibility distribution defines that there must be at least one $\tilde{x}$ such that $\Pi_X(x) = 1$ and this property is known as normalization (Spott 1999). For more details regarding the possibility theory, interested readers are advised to follow (Mujumdar and Ghosh (2008), Das et al. (2018). The uncertainty analysis is carried out at each grid point under 3-, 4-, 6-month scales to access the GCM and scenario uncertainties. In order to satisfy the normalization property, the results obtained from NSE for nineteen GCMs and two scenarios are divided by the maximum NSE value and the normalized value is considered as the possibility value for a corresponding GCM and scenario.

3.4 Formulation of SAF curves for seasonal droughts

The SAF relationship is commonly used to visualize and interpret the drought at regional scale. The SAF curve defines the cumulative drought affected areas for the chosen severity level under different return periods. Therefore, it enables to provide quick and effective interpretation of drought condition in order to take sustainable mitigation measures (Bonaccorso et al. 2015). In this study, the seasons: pre-monsoon, monsoon, post-monsoon, Rabi and Kharif are taken into account for seasonal drought analysis.

It should be noted that the calculation is carried out after performing the GCM and scenario uncertainty. The following steps are employed to derive the SAF curve over the study area: (1) SPEI drought indicator is computed for 3, 4 and 6-month time scales, where 3-month time scale for pre-monsoon, post-monsoon season, 4-month time scale for monsoon and kharif season, and 6-month time scale for rabi season, (2) the drought indicator value less than zero is taken into consideration for the further analysis, (3) the frequency analysis is carried out by considering the non-zero values using extreme value, normal, exponential, gamma, lognormal, and Weibull distributions at each grid point for different drought time scale, (4) the severity as return levels for different return periods such as 5, 10, 25, 50, and 100 are computed using the statistical parameter estimated for the corresponding grid point and suitable distribution, (5) the spatial extent of drought occurrence is computed in terms of percentage of area for different threshold values of drought severity, (6) finally, the values of severity, areal extent, and frequency are linked to construct the SAF curve.

It is worth mentioning that the analysis is carried out over each division. Initially, the weight of each grid point corresponding to any division shapefile is computed. The weight defines the percentage of grid area fall within the division shapefile. For example, if the weight value of a grid is 0.7 (1), then 70% of the grid area (complete grid) comes inside the shapefile. The computation for all the divisions is performed using "raster" package in R developed by Hijmans et al. (2019). The present study considers five different severity values i.e., − 1, − 1.5, − 2, − 2.5, − 3 as threshold to calculate the drought-affected area below the threshold severity level. Moreover, the threshold severity values are interpolated for the drought-affected area using cubic interpolation technique.

In the present study, drought at 3, 4, and 6-month time scales are examined which represent short-term to seasonal drought condition. The analysis would be help in identifying the operational definition of drought i.e. from meteorological to hydrological drought. In particular, 3 to 4-month scale drought conditions highlight the soil moisture condition that would help in guiding the agricultural operation. Similarly, 6-month scale drought condition reflect the hydrological condition depending on the region and time of year.

4 Results

4.1 Bias-correction of NEX-GDDP simulation

The bias-correction of precipitation, Tmax, and Tmin is carried out for 19 NEX-GDDP simulations considering the IMD observations as reference data during 1951–2005 before the computation of SPEI. Moreover, it is well documented that it is necessary to correct the bias in the climate model while projecting future drought events (Wehner et al. 2011). Here, non-parametric quantile mapping is used as bias-correction technique assuming the biases at each quantile as time-invariant or stationary (Maraun et al. 2017).

For brevity, a comparative analysis between the before and after bias-correction of precipitation at a particular grid location (74.875 longitude, 20.625 latitude) is presented in Fig. 3. Similarly, for maximum and minimum temperature, refer to the supplementary Figure S1.

It can be noted from Fig. 3 that there is significant bias associated with the higher quantiles (95th, 99th, and 100th) before the correction. Conversely, it is observed that the bias has reduced after bias-correction for all the GCMs. Similarly, in case of temperature, the range of the bias is more in the case of Tmin than Tmax. In addition, both positive and negative biases for Tmin and only positive bias for Tmax are noticed before bias-correction. It is worth mentioning that the range of the bias is different at different grid points. The bias associated with the future period is corrected using the correction during the baseline period for the three meteorological variables.

4.2 Uncertainty analysis and future projection of meteorological variables

The performance measure NSE is computed for 19 GCMs under RCP4.5 and 8.5 scenarios based on their prediction of SPEI at 3-, 4-, and 6-month time scales in the recent past (from 1993 to 2018). The possibility value is computed by dividing the maximum NSE value. This operation is carried out for each grid point separately. Figure 4 presents the distribution of different GCMs and scenarios across the study area for 3-month time scale. Figures S2 and S3 in supplementary information depict the suitable GCM and scenario for 4- and 6-month scales, respectively. It can be noted that for 3-month scale, RCP4.5 (RCP8.5) scenario is

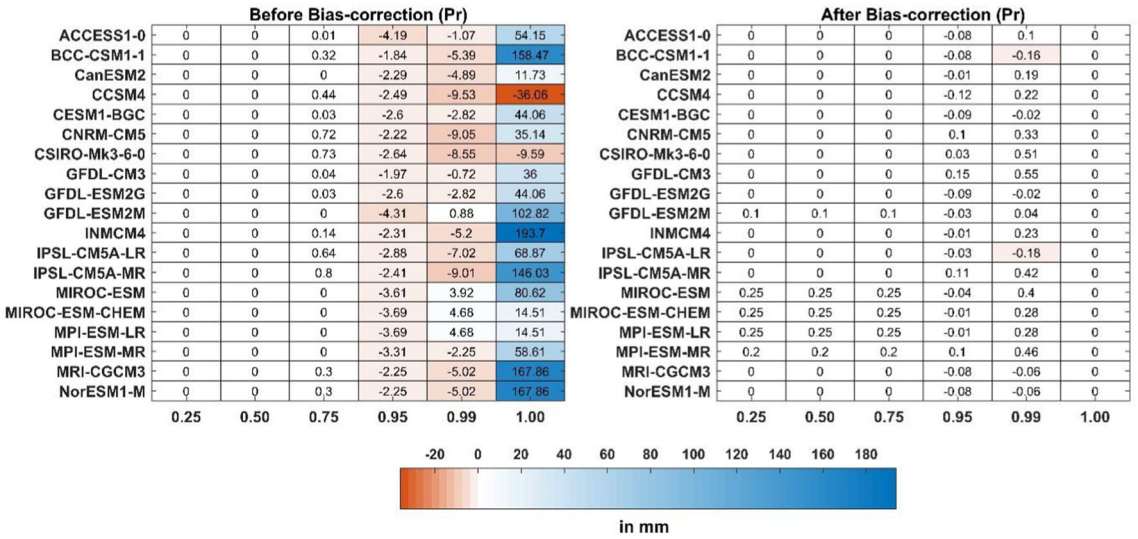

Fig. 3 Before (left) and after (right) bias-correction of precipitation magnitude at different quantiles

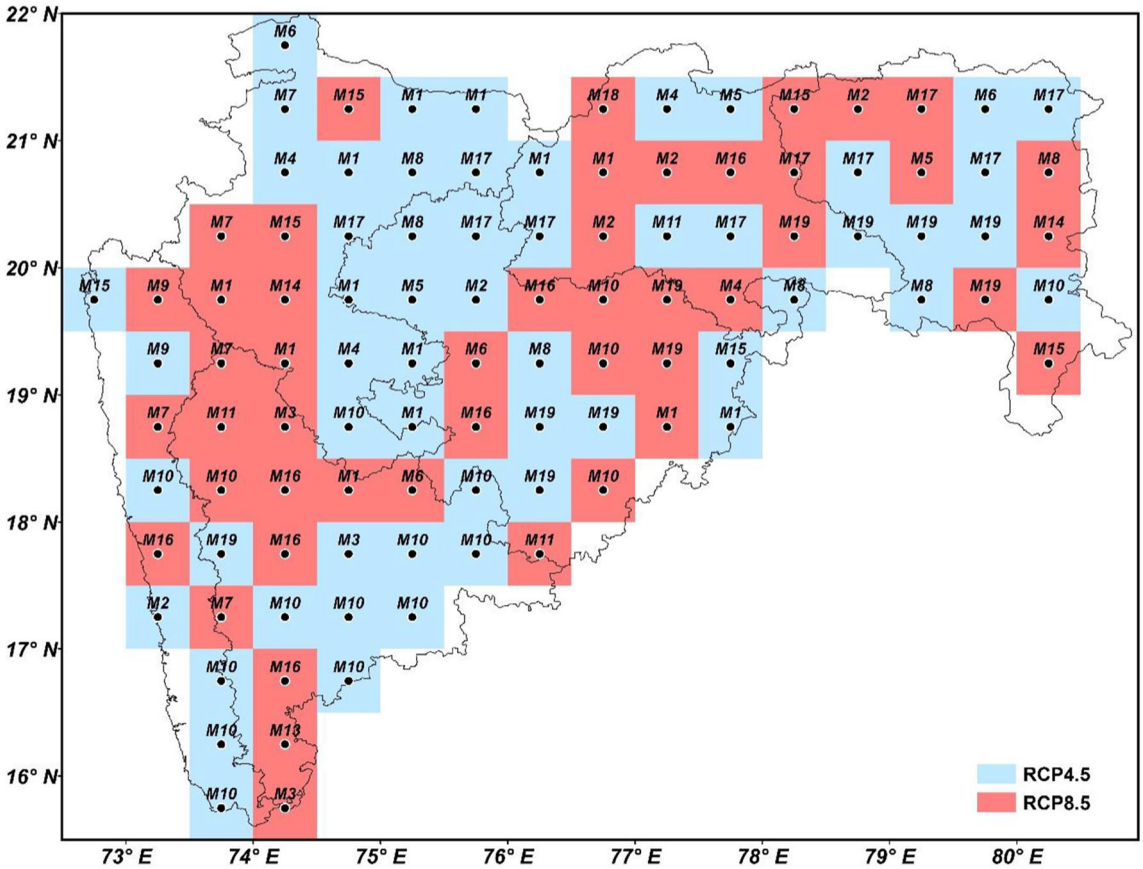

Fig. 4 Most suitable GCM/scenario at each grid point for 3-month time scale SPEI after uncertainty analysis

considered as most possible scenario over 54% (46%) of total grid points. Similarly, most possible scenario for 4-month time scale (6-month scale) is found to be 53% (38%) of total grids for RCP4.5 and 47% (62%) of total grids for RCP8.5.

Considering the most possible GCM and scenario at each grid point, the spatio-temporal variabilities with respect to T0 for different variables such as precipitation, potential evapotranspiration, maximum and minimum temperature are computed and plotted. Figure 5 presents

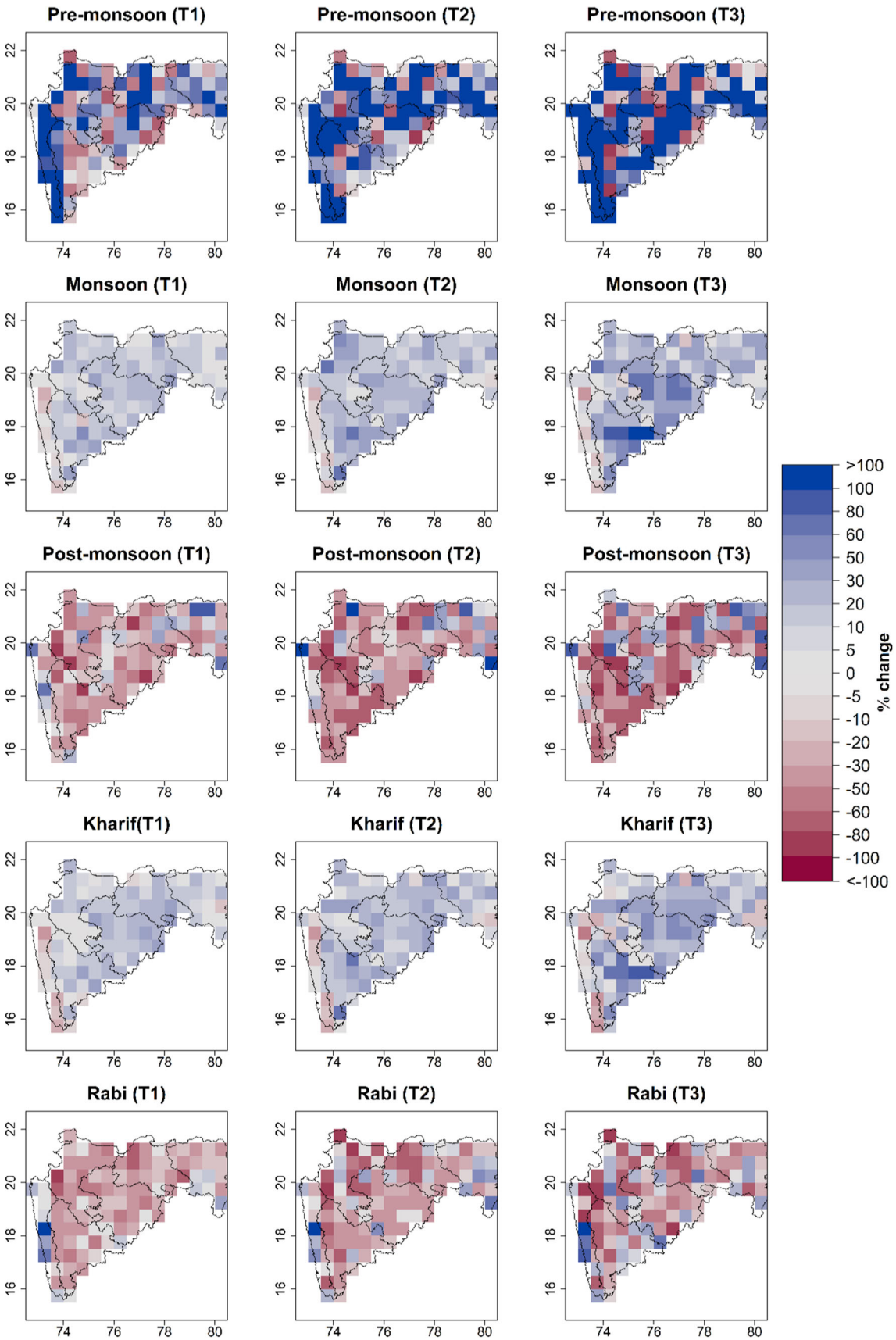
Pre-monsoon (T1)
Pre-monsoon (T2)
Pre-monsoon (T3)
Monsoon (T1)
Monsoon (T2)
Monsoon (T3)
Post-monsoon (T1)
Post-monsoon (T2)
Post-monsoon (T3)
Kharif(T1)
Kharif (T2)
Kharif (T3)
Rabi (T1)
Rabi (T2)
Rabi (T3)
16
18
20
22
74
76
78
80
>100
100
80
60
50
30
20
10
5
0
-5
-10
-20
-30
-50
-60
-80
-100
<-100
% change

◀**Fig. 5** Spatio-temporal variability of precipitation (in percentage) for different seasons

the spatio-temporal variability (% change) of precipitation for different seasons during T1, T2, and T3 time periods. Similarly, Figures S4, S5, and S6 (refer to supplementary information) shows the spatio-temporal variability of potential evapotranspiration, maximum, minimum temperature, respectively. From Fig. 5, it can be noted that the precipitation magnitude is projected to increase (decrease) in pre-monsoon by 65–79% (21–35%), in monsoon by 83–90% (10–17%), in post-monsoon by 18–27% (73–82%), in Kharif by 79–86% (14–21%), in Rabi by 18–29% (71–82%) of total grid area between T1 and T3. In case of potential evapotranspiration, it is projected to increases (decrease) in pre-monsoon by 49–57% (43–51%), in monsoon by 24–44% (56–76%), in post-monsoon by 50–84% (16–50%), in Kharif by 50–69% (31–50%), in Rabi by 69–88% (12–31%) of total area during T1 and T3. However, the future variability in maximum and minimum temperature is expected to increase over most of the gridded area for all the seasons with maximum variability in case of minimum temperature. In addition, it is noticed that the magnitude maximum and minimum temperature is likely to increase from T1 to T3 as compared to T0.

4.3 Seasonal variability of SPEI under climate change

Based on the classification of SPEI (refer to Table 2), moderate, severe, and extreme drought conditions are analysed for future periods and compared with T0. Figure 6 presents the season-wise frequency of different drought conditions across the study area. The red circle in the boxplot represents the mean frequency value. It is noted that the frequency of moderate drought condition (Top panel of Fig. 6) is expected to decrease during Kharif, monsoon, and pre-monsoon seasons as compared to historical period. In case of Rabi season, the mean frequency of moderate drought condition is likely to increase during T1 and decrease gradually in T2 and T3. The mean frequency of severe drought condition is projected to have no significant change in future as compared to T0 during Kharif, monsoon, and pre-monsoon seasons. However, it is likely to increase during post-monsoon and Rabi seasons. The future projection of extreme drought condition shows an increasing frequency in post-monsoon, pre-monsoon, and Rabi seasons, while no change is observed during Kharif and monsoon seasons as compared to T0.

4.4 Analysis of SAF curve over different regions

In this section, SAF curves are analysed over Amaravati, Aurangabad, Konkan, Nagpur, Nashik, and Pune regions for 5-, 10-, 25-, 50-, and 100-year return periods in different seasons and compared with T0 period. It should be noted that the severity return levels are computed using the selected distribution for different return periods. As discussed, five different severity values i.e., − 1, − 1.5, − 2, − 2.5, − 3 are chosen to develop the SAF curve. Here, the results are presented separately for different regions. For brevity, most of the figures (as presented in sub-sections below) are shown in the supplementary material.

4.4.1 SAF curve for Amaravati

Figure 7 shows the area affected by different severity levels under different return periods during pre-monsoon season over Amaravati region. The top, middle, and bottom panels present for T1, T2, and T3 periods, respectively. The black line corresponds to T0 period, red line defines future simulation, and dashed red line represents the 95% confidence interval of future simulation. During pre-monsoon season, in the case of the 5-year return period, the area affected by different severity of drought is likely to increase for all the future time periods as compared to T0. The area affected by the SPEI severity level less than − 1.7 (for 10-year), − 2.3 (for 25-year), − 2.4 (for 50-year), and − 2.9 (for 100-year) is projected to increase during T1, T2, and T3 periods over Amaravati region. In case of monsoon season (refer to Figure S7 (a)), the percentage of area is likely to increase below the SPEI severity level of − 1.2 (for 5-year during all time periods), − 1.3 (for 10-year during T1), − 1.4 (for 10-year during T2), − 1.5 (for 10-year during T3), − 1.7 (for 25-year during T1), − 2.0 (for 25-year during T2), − 2.1(for 25-year during T3), − 1.8 (for 50-year during T1), − 2.2 (for 50-year during T2 and T3), − 1.7 (for 100-year during T1), − 2.3 (for 100-year during T2), and − 1.9 (for 100-year during T3). During post-monsoon season (refer to Figure S7 (b)), the drought affected area is likely to decrease during T1 for all the return periods. Similarly, for T2 and T3 periods, the drought area is projected to decrease for high return period severity values as compared to T0. In the case of Kharif season (refer to Figure S7 (c)), the projected drought area is likely to increase over more severe drought conditions for all the return periods and future time steps. Most of the cases in Rabi season (refer to Figure S7 (d)), the projected drought-prone area is likely to increase for different severity levels during the twenty-first century.

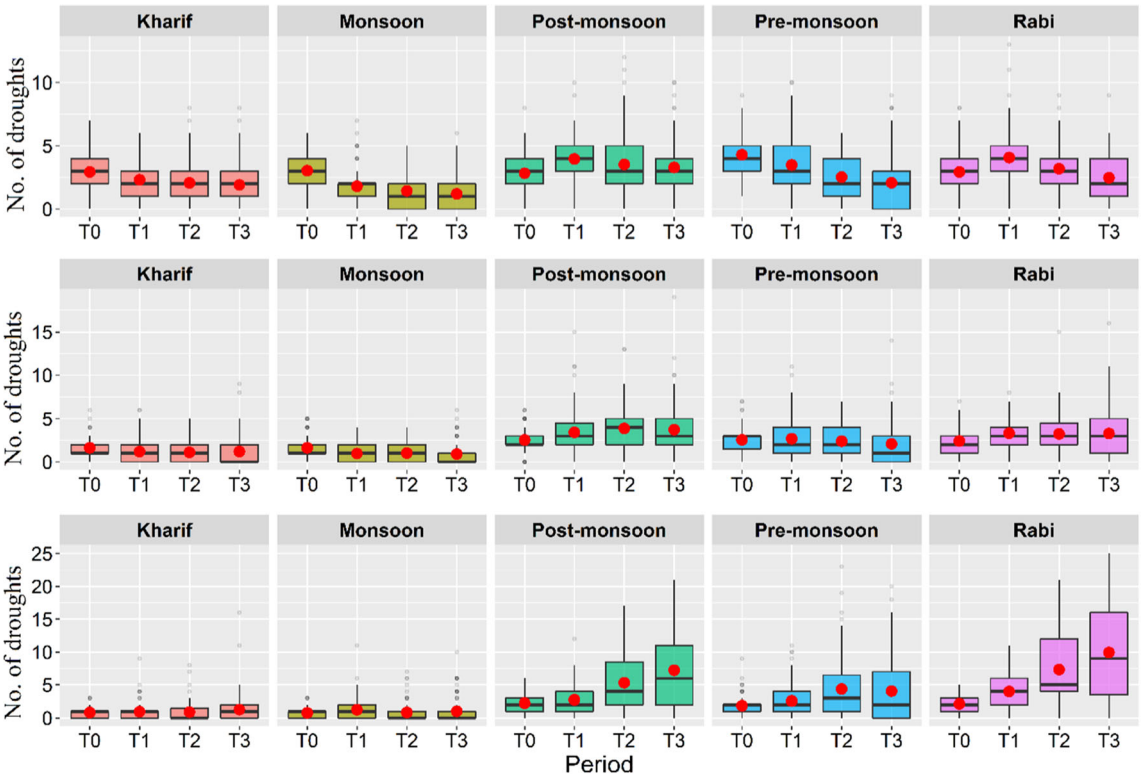

Fig. 6 Total number of drought events under different periods for moderate (upper), severe (middle), and extreme (lower) drought conditions

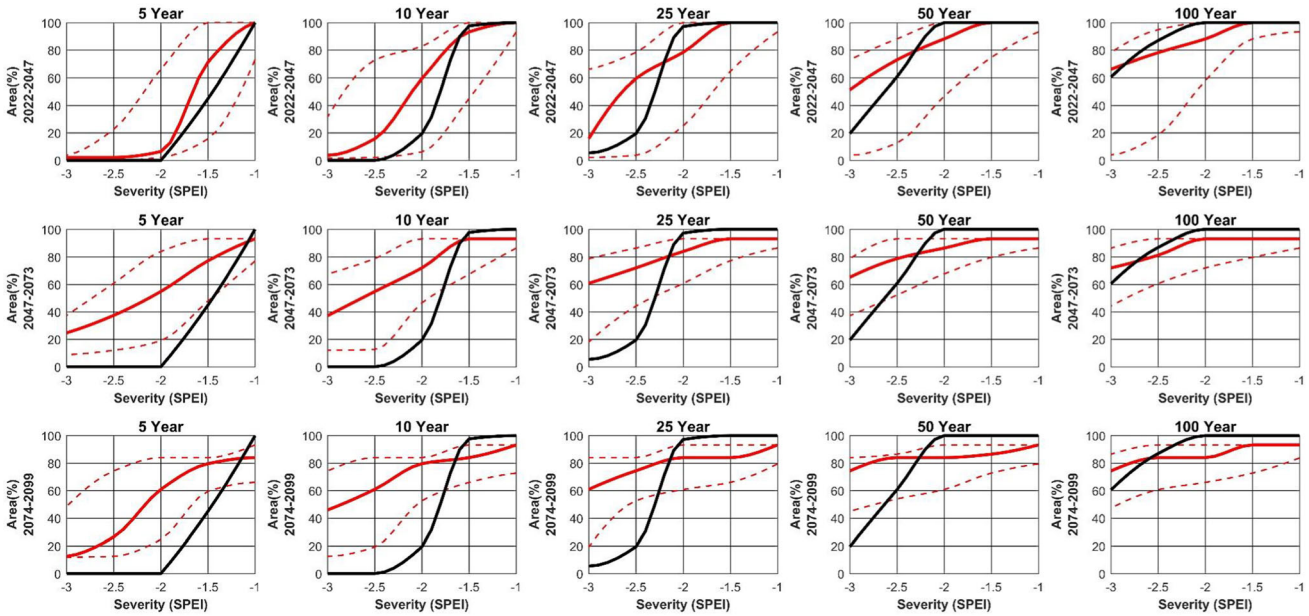

Fig. 7 SAF curve for pre-monsoon season over Amaravati region. The top, middle, and bottom panels present for T1, T2, and T3 periods, respectively. The black line corresponds to T0 period, red line defines future simulation, and dashed red line represents the 95% confidence interval of future simulation

4.4.2 SAF curve for Aurangabad

The SAF curve related to the Aurangabad division is presented in Figure S8. Figure S8 (a) describes the SAF curve for pre-monsoon season. It can be noted that for more severe drought condition, the percentage of affected area is likely to increase for all return periods and future time steps as compared to T0. For 50- and 100-year return periods, the

entire area is projected to affect by the drought severity between − 1.5 and − 1. The SAF curve for monsoon season is presented in Figure S8 (b). For the future time period T2, for most of the return periods, it is observed that the projected drought-affected area for different severity levels is likely to decrease. In the case of T1 period, for more severe condition the percentage of area is expected to increase. For 50- and 100-year return periods, the drought-affected area is reduced significantly during T3 as compared to T0. Figure S8 (c) and (e) present the SAF curves for post-monsoon and Rabi seasons. It can be observed that for both the seasons that the projected drought areas under different severity levels are expected to increase for all return periods and future time steps. However, in the Kharif season (Figure S8 (d)), the future projected SAF curves under most of the return periods and time steps are likely to be less severe than T0.

4.4.3 SAF curve for Konkan

The seasonal SAF curve for the Konkan region is presented in Figure S9. Figure S9 (a), (b), (c), (d), and (e) denote pre-monsoon, monsoon, post-monsoon, Kharif, and Rabi seasons, respectively. The future projected SAF curves are likely to decrease as compared to T0 for most of the return periods in pre-monsoon season. During monsoon season, the future drought-prone area may increase for more severe drought conditions under high return periods. For the severity level less than − 1.8, the drought-affected area is likely to increase as compared to T0. In most of the cases, an increase in drought-affected area is observed during post-monsoon season. With increase in the return period, the area under the drought is likely to decrease in Kharif season. For higher return period, the area under the severe drought condition is expected to increase. During Rabi season, the SAF curves for 50- and 100-year return periods and all future time steps are projected to decrease as compared to T0. In case of T1 time step, the drought-affected area for most of the severity levels is likely to reduce. However, the percentage of area under drought may increase for the severity level less than − 2.0 during T2, and T3 periods under 5- and 10-year return periods.

4.4.4 SAF curve for Nagpur

The SAF curve for the Nagpur region is shown in Figure S10. The pre-monsoon SAF curve (Figure S10 (a)) shows an increase in the percentage drought area in T2 future period. The difference between future simulated and observed SAF curve is larger during T3 than T1. During Monsoon season (Figure S10 (b)), it is observed that 0% area is affected by drought for severity level less than − 2.5 for 5- and 10-year return periods in future. The future SAF curve under 100-year return period during T2 and T3 time steps is likely to decrease as compared to T0. In most of the cases the future simulated area under drought is expected to decrease in post-monsoon season (Figure S10 (c)). In Kharif season (Figure S10 (d)), for most of the return periods, the percentage area increases (decreases) for high (low) severity level as compared to T0. During T1 and T2, the area under drought is projected to decrease under 100-year return period. However, the areal drought condition may increase during Rabi season under all the return periods in future.

4.4.5 SAF curve for Nashik

Figure S11 depicts the SAF curve for Nashik region. In pre-monsoon season (Figure S11 (a)), the increment in future projected drought-prone area is observed under all the return periods for T1 time step. During T2 period, with increase in return period, the area under drought is shifted towards the more severe drought condition. A similar kind of observation is also noticed in case of T3 period. During monsoon season, in most of the cases the percentage of areal drought has increased as compared to T0 in different return periods (Figure S11 (b)). The post-monsoon season (Figure S11 (c)) shows less variability in case of 25-, 50-, and 100-year return periods. In general, the projected drought area is expected to increase during the season. In Kharif season (Figure S11 (d)), a significant increment in the areal coverage of drought is observed for all the return periods during T3 as compared to T1 and T2. Similar to Nagpur region, the areal drought condition may increase during Rabi season under all the return periods in future (Figure S11 (e)).

4.4.6 SAF curve for Pune

For Pune region, the SAF curve is presented in Figure S12. It is noticed that the area under the drought is likely to decrease during pre-monsoon season (Figure S12 (a)) under high return period. However, during T2 period, the drought-affected area for more severe drought condition may increase under 5- and 10-year return periods. A gradual decrease in the drought area is expected in future with increase in the return period during monsoon season (Figure S12 (b)). However, it is observed that the SAF curves for all the return period are likely to increase in all future periods as compared to T0 during post-monsoon season (Figure S12 (c)). In Kharif season (Figure S12 (d)), at high return levels the drought-affected areas are likely to decrease for all the future time steps. However, for 5-, 10-, and 25-year return periods, the SAF curve is likely to increase for severe drought conditions in future. Similar to post-monsoon season, the areal drought condition may

increase during Rabi season under all the return periods in future (Figure S12 (e)).

4.5 Changes in future drought-affected area

The changes in drought-affected areas are plotted using heatmaps. Figure 8 presents the percentage in the drought-affected area in different seasons with respect to T0 period. The upper panel defines Amaravati region and lower panel refers to Aurangabad region. Similarly, Figures S13 and S14 present the percentage area change for Konkan (upper panel), Nagpur (lower panel), and Nashik (upper panel), Pune (lower panel), respectively. It can be noted that for higher magnitude of drought severity the percentage area under different return periods is likely to increase for Amaravati. The increment in the drought prone area is observed in case of pre-monsoon and Rabi seasons for Amaravati and Aurangabad divisions. However, there will be significant decrement or no significant change in drought-affected area for lower magnitude of drought severity. In a similar way, in Konkan division, there is no sign of increment in drought-affected area during pre-monsoon season. However, during other seasons, there is a significant increase in drought-affected area for extreme drought condition except for T1 future period during Rabi season. Likewise, in Nagpur, pre-monsoon and Rabi seasons and in Pune, post-monsoon and Rabi seasons are comparatively more affected by drought in future time periods. However, as compared to other divisions, Nashik is likely deal with the increment in drought-affected area during most of the seasons in future as compared to T0 period.

5 Discussion and conclusions

The concurrent variability in hydro-meteorological variables makes it difficult to understand the regional drought severity during different seasons. Hence, analysing the seasonal drought characteristics under the influence of climate change needs to be examined. The present study makes an attempt understand the drought attributes during different seasons by developing and comparing the SAF relationship for historical and future periods. The future meteorological outputs from 19 NEX-GDDP simulations under two emission scenarios are used. Prior to the analysis, uncertainty associated with GCM and scenario is analysed using the possibility theory. Based on the analysis, the most possible GCM and scenario at each grid point for 3-, 4-, and 6-month time scale are selected. It should be noted that the GCM/scenario with a possibility value of 1 does not mean that the selected GCM/scenario perfectly projects the climate change at that particular grid. However, it denotes the nonexistence of any better GCM/scenario to capture the climate change variability at that grid point. The future temperature for all the seasons and precipitation for pre-monsoon, monsoon, and Kharif seasons are expected to increase. The warming and wetting nature of the climate during the twenty-first century is in line with TERI (2014). In addition, the increase over the study area

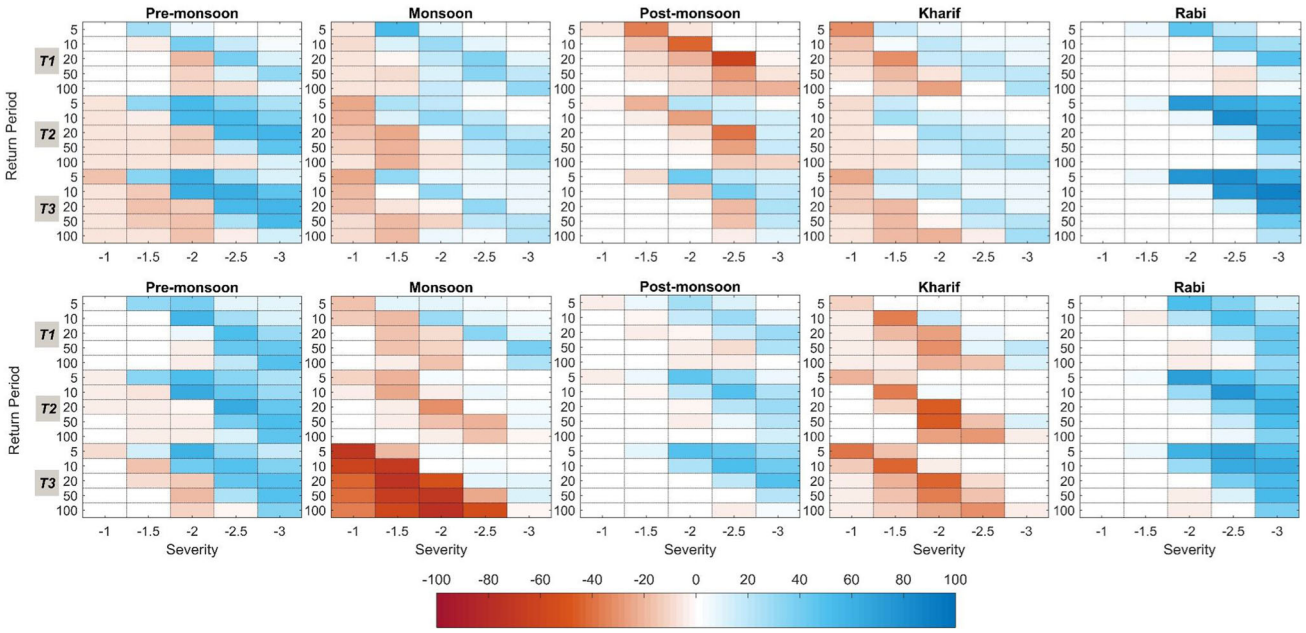

Fig. 8 Heatmaps showing percentage change in drought areal extent for Amaravati (upper) and Aurangabad (lower) divisions under different seasons

can be attributed to the increasing rate of global warming (Yaduvanshi et al. 2019). Therefore, the spatio-temporal variability of meteorological variables can cause shift in water balance over and under the ground.

The evaluation of drought SAF relationship curves for analysing drought characteristics enable to compare the drought attributes during each season across the study area during. During T0 period, it can be clearly distinguished from the SAF curve that mild drought conditions with less severity i.e., SPEI value between − 1.5 and − 1.0 cover more area for each return period. However, in most of the cases in future period, the SAF curves for different seasons indicate increase in area with severity magnitude less than equal to − 2.0. The outcomes manifest that the study area is sensitive towards extreme drought occurrences. Additionally, higher return period covers more area as compared to lower return period.

The outcomes obtained from this study confirm similar types of findings resulted from previous studies based on seasonal drought analysis associated with different range of drought severity and return periods for evaluating drought-affected areas. Ahmed et al. (2019) reported that large areas were drought-affected in Pakistan for higher return period by assessing the drought characteristics with the use of SAF curves. Drought characteristics vary regionally depending on its geographic and climatic condition. In addition, the uncertainties in drought-affected areas may arise due to the differences in methodologies, variation in data obtained from different sources including GCMs. Therefore, drought characteristics have been calculated here per division wise for better understanding which appears to be more useful to improve the socio-economic condition in Maharashtra.

From the analysis of drought characteristics among all seasons across each division of Maharashtra, it is observed that there is an increment in percentage of the drought-affected area especially for the higher magnitude of severity in future period. Previous studies have already reported about the increment in drought-affected area with long term and severe droughts in different parts of the world (Amirataee et al. 2018; Himayoun and Roshni 2019). In addition, it has also been suggested from recent studies that the drought events with rise in severity and frequency will continuously increase in many regions across the world in coming decades due to projected climate change factors (Sharma and Mujumdar 2017; Bisht et al. 2019). Specifically, the regions with frequent drought events will be highly prone to future drought occurrences due to climate change scenarios (Kundzewicz et al. 2008). On this account, the present study has also revealed that the increased drought occurrences with large spatial extent suffering from severe and extreme drought conditions in each division for future time series. With this understanding, the key outcomes from the present analysis are as follows:

- The precipitation magnitude is expected to increase in pre-monsoon, monsoon, and Kharif seasons over most of the areas in Maharashtra. Except for monsoon season, the potential evapotranspiration is projected to increase over 50% of the total area.
- Increase in the temperature profile is noticed over all the regions in Maharashtra during the twenty-first century.
- The extreme drought condition during post-monsoon, pre-monsoon and Rabi seasons shows an increase in the frequency as compared to historical period.
- The SAF curve reveals that, in most of the cases, the percentage of drought-affected area is expected to increase for high magnitude of severity. In addition, the highest increment in the drought-affected area is observed during the Rabi season in future.

The future study can be undertaken to analyse the different types of drought such as hydrological, agricultural, and socio-economic to provide better assessment regarding drought characteristics and identification of the regional distribution of risk associated with drought.

Declarations

Conflict of interest The authors declare that there is no known conflict of interest to influence the work reported in the submitted manuscript.

References

Aadhar S, Mishra V (2018) Impact of climate change on drought frequency over India. B Clim Chang Water Resour India Publ Minist Environ For Clim Chang (MoEF&CC), Gov India, New Delhi

Aadhar S, Mishra V (2020) Increased drought risk in South Asia under warming climate: implications of uncertainty in potential evapotranspiration estimates. J Hydrometeorol. https://doi.org/10.1175/JHM-D-19-0224.1

AghaKouchak A, Feldman D, Hoerling M et al (2015) Water and climate: recognize anthropogenic drought. Nature 524:409–411. https://doi.org/10.1038/524409a

Ahmadalipour A, Moradkhani H, Svoboda M (2017) Centennial drought outlook over the CONUS using NASA-NEX downscaled climate ensemble. Int J Climatol 37:2477–2491. https://doi.org/10.1002/joc.4859

Ahmed K, Shahid S, Chung ES et al (2019) Climate change uncertainties in seasonal drought severity-area-frequency curves: case of arid region of Pakistan. J Hydrol. https://doi.org/10.1016/j.jhydrol.2019.01.019

Allen RG, Smith M, Pereira LS, Perrier A (1994) An update for the calculation of reference evapotranspiration. ICID Bull 43:35–92

Amarasinghe U, Amarnath G, Alahacoon N, Ghosh S (2020) How do floods and drought impact economic growth and human development at the sub-national level in India? Climate 8:123. https://doi.org/10.3390/cli8110123

Amirataee B, Montaseri M, Rezaie H (2018) Regional analysis and derivation of copula-based drought severity-area-frequency curve in Lake Urmia basin, Iran. J Environ Manag. https://doi.org/10.1016/j.jenvman.2017.10.027

Ashfaq M, Bowling LC, Cherkauer K et al (2010) Influence of climate model biases and daily-scale temperature and precipitation events on hydrological impacts assessment: a case study of the United States. J Geophys Res 115:D14116. https://doi.org/10.1029/2009JD012965

Bandyopadhyay A, Bhadra A, Swarnakar RK et al (2012) Estimation of reference evapotranspiration using a user-friendly decision support system: DSS_ET. Agric Meteorol 154–155:19–29. https://doi.org/10.1016/j.agrformet.2011.10.013

Beguería S, Vicente-Serrano SM, Reig F, Latorre B (2014) Standardized precipitation evapotranspiration index (SPEI) revisited: parameter fitting, evapotranspiration models, tools, datasets and drought monitoring. Int J Climatol 34:3001–3023. https://doi.org/10.1002/joc.3887

Begueria S, Serrano V, Sawasawa H (2017) Calculation of the standardised precipitation-evapotranspiration index. R-Package

Bisht DS, Sridhar V, Mishra A et al (2019) Drought characterization over India under projected climate scenario. Int J Climatol 39:1889–1911. https://doi.org/10.1002/joc.5922

Bonaccorso B, Peres DJ, Castano A, Cancelliere A (2015) SPI-based probabilistic analysis of drought areal extent in Sicily. Water Resour Manag 29:459–470. https://doi.org/10.1007/s11269-014-0673-4

Burke EJ, Brown SJ (2008) Evaluating uncertainties in the projection of future drought. J Hydrometeorol 9:292–299. https://doi.org/10.1175/2007JHM929.1

Chen S, Liu W, Ye T (2020) Dataset of trend-preserving bias-corrected daily temperature, precipitation and wind from NEX-GDDP and CMIP5 over the Qinghai-Tibet Plateau. Data Br 31:105733. https://doi.org/10.1016/j.dib.2020.105733

Christensen OB, Gaertner MA, Prego JA, Polcher J (2001) Internal variability of regional climate models. Clim Dyn 17:875–887. https://doi.org/10.1007/s003820100154

Dai A (2011a) Drought under global warming: a review. Wiley Interdiscip Rev Clim Chang 2:45–65. https://doi.org/10.1002/wcc.81

Dai A (2011b) Characteristics and trends in various forms of the Palmer Drought Severity Index during 1900–2008. J Geophys Res Atmos. https://doi.org/10.1029/2010JD015541

Dai A, Zhao T, Chen J (2018) Climate change and drought: a precipitation and evaporation perspective. Curr Clim Chang Rep 4:301–312. https://doi.org/10.1007/s40641-018-0101-6

Das J, Umamahesh NV (2018) Assessment of uncertainty in estimating future flood return levels under climate change. Nat Hazards. https://doi.org/10.1007/s11069-018-3291-2

Das J, Treesa A, Umamahesh NV (2018) Modelling impacts of climate change on a river basin: analysis of uncertainty using REA & possibilistic approach. Water Resour Manag. https://doi.org/10.1007/s11269-018-2046-x

Das J, Jha S, Goyal MK (2020a) Non-stationary and copula-based approach to assess the drought characteristics encompassing climate indices over the Himalayan states in India. J Hydrol. https://doi.org/10.1016/j.jhydrol.2019.124356

Das J, Poonia V, Jha S, Goyal MK (2020b) Understanding the climate change impact on crop yield over Eastern Himalayan Region: ascertaining GCM and scenario uncertainty. Theor Appl Climatol 142:467–482. https://doi.org/10.1007/s00704-020-03332-y

Das S, Das J, Umamahesh NV (2021a) Identification of future meteorological drought hotspots over Indian region: a study based on NEX-GDDP data. Int J Climatol. https://doi.org/10.1002/joc.7145

Das S, Das J, Umamahesh NV (2021b) Nonstationary modeling of meteorological droughts: application to a region in India. J Hydrol Eng 26:05020048. https://doi.org/10.1061/(ASCE)HE.1943-5584.0002039

Dubois D (2006) Possibility theory and statistical reasoning. Comput Stat Data Anal 51:47–69. https://doi.org/10.1016/j.csda.2006.04.015

Eden JM, Widmann M, Grawe D, Rast S (2012) Skill, correction, and downscaling of GCM-simulated precipitation. J Clim 25:3970–3984. https://doi.org/10.1175/JCLI-D-11-00254.1

Fischer R, Nowicki S, Kelley M, Schmidt GA (2014) A system of conservative regridding for ice-atmosphere coupling in a general circulation model (GCM). Geosci Model Dev 7:883–907. https://doi.org/10.5194/gmd-7-883-2014

Ghosh S, Mujumdar PP (2009) Climate change impact assessment: uncertainty modeling with imprecise probability. J Geophys Res 114:D18113. https://doi.org/10.1029/2008JD011648

Giorgi F, Mearns LO (2003) Probability of regional climate change based on the reliability ensemble averaging (REA) method. Geophys Res Lett. https://doi.org/10.1029/2003GL017130

Gore PG, Ray KC (2002) Variability in drought incidence over districts of Maharashtra. Mausam 53(4):533–538

Gudmundsson L (2016) Statistical transformations for post-processing climate model output. Tech Rep. https://doi.org/10.5194/hess-16-3383-2012.bernexp

Gudmundsson L, Bremnes JB, Haugen JE, Engen-Skaugen T (2012) Technical note: downscaling RCM precipitation to the station scale using statistical transformations—a comparison of methods. Hydrol Earth Syst Sci. https://doi.org/10.5194/hess-16-3383-2012

Hargreaves GH (1994) Defining and using reference evapotranspiration. J Irrig Drain Eng. https://doi.org/10.1061/(asce)0733-9437(1994)120:6(1132)

Henriques AG, Santos MJJ (1999) Regional drought distribution model. Phys Chem Earth Part B Hydrol Ocean Atmos. https://doi.org/10.1016/S1464-1909(98)00005-7

Her Y, Yoo SH, Cho J et al (2019) Uncertainty in hydrological analysis of climate change: multi-parameter vs. multi-GCM ensemble predictions. Sci Rep. https://doi.org/10.1038/s41598-019-41334-7

Hewitson BC, Daron J, Crane RG et al (2014) Interrogating empirical-statistical downscaling. Clim Chang 122:539–554. https://doi.org/10.1007/s10584-013-1021-z

Hijmans RJ, van Etten J, Sumner M et al (2019) Package raster: geographic data analysis and modeling

Himayoun D, Roshni T (2019) Spatio-temporal variation of drought characteristics, water resource availability and the relation of drought with large scale climate indices: a case study of Jhelum basin, India. Quat Int. https://doi.org/10.1016/j.quaint.2019.07.018

Höllermann B, Evers M (2017) Perception and handling of uncertainties in water management—a study of practitioners' and scientists' perspectives on uncertainty in their daily decision-making. Environ Sci Policy 71:9–18. https://doi.org/10.1016/j.envsci.2017.02.003

Jain S, Salunke P, Mishra SK et al (2019) Advantage of NEX-GDDP over CMIP5 and CORDEX data: Indian summer monsoon. Atmos Res 228:152–160. https://doi.org/10.1016/j.atmosres.2019.05.026

Jha S, Das J, Goyal MK (2019) Assessment of risk and resilience of terrestrial ecosystem productivity under the influence of extreme

climatic conditions over India. Sci Rep. https://doi.org/10.1038/s41598-019-55067-0
Kelkar SM, Kulkarni A, Rao KK (2020) Impact of climate variability and change on crop production in Maharashtra, India. Curr Sci 118:1235–1245. https://doi.org/10.18520/cs/v118/i8/1235-1245
Kew S, Philip S, Hauser M et al (2019) Impact of precipitation and increasing temperatures on drought in eastern Africa. Earth Syst Dyn Discuss. https://doi.org/10.5194/esd-2019-20
Khadr M (2017) Temporal and spatial analysis of meteorological drought characteristics in the upper Blue Nile river region. Hydrol Res 48:265–276. https://doi.org/10.2166/nh.2016.194
Khan N, Shahid S, Ahmed K et al (2018) Performance assessment of general circulation model in simulating daily precipitation and temperature using multiple gridded datasets. Water Switz. https://doi.org/10.3390/w10121793
Khan N, Shahid S, Ahmed K et al (2020) Selection of GCMs for the projection of spatial distribution of heat waves in Pakistan. Atmos Res. https://doi.org/10.1016/j.atmosres.2019.104688
Kundzewicz ZW, Mata LJ, Arnell NW et al (2008) The implications of projected climate change for freshwater resources and their management. Hydrol Sci J. https://doi.org/10.1623/hysj.53.1.3
Lafon T, Dadson S, Buys G, Prudhomme C (2013) Bias correction of daily precipitation simulated by a regional climate model: a comparison of methods. Int J Climatol. https://doi.org/10.1002/joc.3518
Leander R, Buishand TA (2007) Resampling of regional climate model output for the simulation of extreme river flows. J Hydrol 332:487–496. https://doi.org/10.1016/j.jhydrol.2006.08.006
Lenderink G, Buishand A, Van Deursen W (2007) Estimates of future discharges of the river Rhine using two scenario methodologies: direct versus delta approach.https://doi.org/10.5194/hess-11-1145-2007
Lester R, Gurenko E (2003) Financing rapid onset natural disaster losses in India: a risk management approach. Technical paper. World Bank, Washington, DC
Li Z, Shao Q, Tian Q, Zhang L (2020) Copula-based drought severity-area-frequency curve and its uncertainty, a case study of Heihe River basin, China. Hydrol Res 51:867–881. https://doi.org/10.2166/nh.2020.173
Lin H, Wang J, Li F et al (2020) Drought trends and the extreme drought frequency and characteristics under climate change based on spi and hi in the upper and middle reaches of the Huai River Basin. China Water Switz. https://doi.org/10.3390/W12041100
Lloyd-Hughes B (2014) The impracticality of a universal drought definition. Theor Appl Climatol 117:607–611. https://doi.org/10.1007/s00704-013-1025-7
Maraun D, Shepherd TG, Widmann M et al (2017) Towards process-informed bias correction of climate change simulations. Nat Clim Chang 7:764–773. https://doi.org/10.1038/nclimate3418
Mearns LO, Rosenzweig C, Goldberg R (1996) The effect of changes in daily and interannual climatic variability on ceres-wheat: a sensitivity study. Clim Chang 32:257–292. https://doi.org/10.1007/BF00142465
Milly PCD, Dunne KA (2016) Potential evapotranspiration and continental drying. Nat Clim Chang 6:946–949. https://doi.org/10.1038/nclimate3046
Mishra AK, Singh VP (2009) Analysis of drought severity-area-frequency curves using a general circulation model and scenario uncertainty. J Geophys Res Atmos. https://doi.org/10.1029/2008JD010986
Mishra AK, Singh VP (2010) A review of drought concepts. J Hydrol 391:202–216. https://doi.org/10.1016/j.jhydrol.2010.07.012
Mishra V, Shah R, Thrasher B (2014) Soil moisture droughts under the retrospective and projected climate in India. J Hydrometeorol. https://doi.org/10.1175/JHM-D-13-0177.1
Mishra V, Tiwari AD, Aadhar S et al (2019) Drought and famine in India, 1870–2016. Geophys Res Lett 46:2075–2083. https://doi.org/10.1029/2018GL081477
Mujumdar PP, Ghosh S (2008) Modeling GCM and scenario uncertainty using a possibilistic approach: application to the Mahanadi River, India. Water Resour Res. https://doi.org/10.1029/2007WR006137
Najafi R, Hessami Kermani MR (2017) Uncertainty modeling of statistical downscaling to assess climate change impacts on temperature and precipitation. Water Resour Manag 31:1843–1858. https://doi.org/10.1007/s11269-017-1615-8
New M, Hulme M (2000) Representing uncertainty in climate change scenarios: a Monte-Carlo approach. Integr Assess 1:203–213. https://doi.org/10.1023/A:1019144202120
Pai DS, Sridhar L, Rajeevan M et al (2014) Development of a new high spatial resolution (0.25° × 0.25°) long period (1901–2010) daily gridded rainfall data set over India and its comparison with existing data sets over the region. Mausam 65:1–18
Peng S, Ding Y, Liu W, Li Z (2019) 1 km monthly temperature and precipitation dataset for China from 1901 to 2017. Earth Syst Sci Data 11:1931–1946. https://doi.org/10.5194/essd-11-1931-2019
Piani C, Haerter JO, Coppola E (2010) Statistical bias correction for daily precipitation in regional climate models over Europe. Theor Appl Climatol 99:187–192. https://doi.org/10.1007/s00704-009-0134-9
Poonia V, Jha S, Goyal MK (2021a) Copula based analysis of meteorological hydrological and agricultural drought characteristics across Indian river basins. Int J Clim 41(9):4637–4652. https://doi.org/10.1002/joc.7091
Poonia V, Goyal MK, Gupta BB, Gupta AK, Jha S, Das J (2021b) Drought occurrence in different river basins of India and blockchain technology based framework for disaster management. J Clean Prod 312: https://doi.org/10.1016/j.jclepro.2021.127737
Reddy MJ, Ganguli P (2013) Spatio-temporal analysis and derivation of copula-based intensity-area-frequency curves for droughts in western Rajasthan (India). Stoch Environ Res Risk Assess 27:1975–1989. https://doi.org/10.1007/s00477-013-0732-z
ASSOCHAM Report (2016) Drought situation to cost Rs 6.5 lakh crore to economy
Rind D, Goldberg R, Hansen J et al (1990) Potential evapotranspiration and the likelihood of future drought. J Geophys Res. https://doi.org/10.1029/jd095id07p09983
Sachindra DA, Huang F, Barton A, Perera BJC (2013) Least square support vector and multi-linear regression for statistically downscaling general circulation model outputs to catchment streamflows. Int J Climatol 33:1087–1106. https://doi.org/10.1002/joc.3493
Sahany S, Mishra SK, Salunke P (2019) Historical simulations and climate change projections over India by NCAR CCSM4: CMIP5 vs. NEX-GDDP. Theor Appl Climatol 135:1423–1433. https://doi.org/10.1007/s00704-018-2455-z
Shackley S, Young P, Parkinson S, Wynne B (1998) Uncertainty, complexity and concepts of good science in climate change modelling: are GCMs the best tools? Clim Chang 38:159–205. https://doi.org/10.1023/A:1005310109968
Shah D, Mishra V (2020) Integrated drought index (IDI) for drought monitoring and assessment in India. Water Resour Res. https://doi.org/10.1029/2019WR026284
Sharma A, Goyal MK (2020) Assessment of drought trend and variability in India using wavelet transform. Hydrol Sci J 65:1539–1554. https://doi.org/10.1080/02626667.2020.1754422
Sharma S, Mujumdar P (2017) Increasing frequency and spatial extent of concurrent meteorological droughts and heatwaves in India. Sci Rep 7:15582. https://doi.org/10.1038/s41598-017-15896-3

Sheffield J, Wood EF (2012) Drought: past problems and future scenarios. Routledge, London

Sheffield J, Goteti G, Wood EF (2006) Development of a 50-year high-resolution global dataset of meteorological forcings for land surface modeling. J Clim 19:3088–3111. https://doi.org/10.1175/JCLI3790.1

Shivam GMK, Sarma AK (2017) Analysis of the change in temperature trends in Subansiri River basin for RCP scenarios using CMIP5 datasets. Theor Appl Climatol 129:1175–1187. https://doi.org/10.1007/s00704-016-1842-6

Singh V, Jain SK, Singh PK (2019) Inter-comparisons and applicability of CMIP5 GCMs, RCMs and statistically downscaled NEX-GDDP based precipitation in India. Sci Total Environ. https://doi.org/10.1016/j.scitotenv.2019.134163

Spinoni J, Vogt JV, Naumann G et al (2018) Will drought events become more frequent and severe in Europe? Int J Climatol 38:1718–1736. https://doi.org/10.1002/joc.5291

Spinoni J, Barbosa P, Bucchignani E et al (2019) Future global meteorological drought hotspots: a study based on CORDEX data. J Clim. https://doi.org/10.1175/JCLI-D-19-0084.1

Spinoni J, Barbosa P, Bucchignani E et al (2020) Future global meteorological drought hot spots: a study based on CORDEX data. J Clim. https://doi.org/10.1175/JCLI-D-19-0084.1

Spott M (1999) A theory of possibility distributions. Fuzzy Sets Syst 102:135–155. https://doi.org/10.1016/S0165-0114(97)00102-4

Srivastava AK, Rajeevan M, Kshirsagar SR (2009) Development of a high resolution daily gridded temperature data set (1969–2005) for the Indian region. Atmos Sci Lett. https://doi.org/10.1002/asl.232

Svoboda M, LeComte D, Hayes M et al (2002) The drought monitor. Bull Am Meteorol Soc 83:1181–1190. https://doi.org/10.1175/1520-0477(2002)083%3c1181:TDM%3e2.3.CO;2

Tallaksen LM, Van Lanen HAJ (2004) Hydrological drought: processes and estimation methods for streamflow and groundwater

TERI (2014) Assessing climate change vulnerability and adaptation strategies for Maharashtra: Maharashtra state adaptation action plan on climate change (MSAAPC). TERI, New Delhi

Teutschbein C, Seibert J (2013) Is bias correction of regional climate model (RCM) simulations possible for non-stationary conditions? Hydrol Earth Syst Sci 17:5061–5077. https://doi.org/10.5194/hess-17-5061-2013

Thornthwaite CW (1948) An approach toward a rational classification of climate. Geogr Rev 38:55. https://doi.org/10.2307/210739

Thrasher B, Xiong J, Wang W et al (2013) Downscaled climate projections suitable for resource management. Eos, Trans Am Geophys Union 94:321–323. https://doi.org/10.1002/2013EO370002

Trenberth KE, Dai A, Van Der Schrier G et al (2014) Global warming and changes in drought. Nat Clim Chang 4:17–22. https://doi.org/10.1038/nclimate2067

Udmale P, Ichikawa Y, Manandhar S et al (2014) Farmers' perception of drought impacts, local adaptation and administrative mitigation measures in Maharashtra State, India. Int J Disaster Risk Reduct 10:250–269. https://doi.org/10.1016/j.ijdrr.2014.09.011

Van Loon AF, Gleeson T, Clark J et al (2016) Drought in the Anthropocene. Nat Geosci 9:89–91. https://doi.org/10.1038/ngeo2646

Vicente-Serrano SM, Beguería S, López-Moreno JI (2010) A multiscalar drought index sensitive to global warming: the standardized precipitation evapotranspiration index. J Clim 23:1696–1718. https://doi.org/10.1175/2009JCLI2909.1

Wehner M, Easterling DR, Lawrimore JH et al (2011) Projections of future drought in the continental United States and Mexico. J Hydrometeorol 12:1359–1377. https://doi.org/10.1175/2011JHM1351.1

Yaduvanshi A, Zaroug M, Bendapudi R, New M (2019) Impacts of 15 °C and 2 °C global warming on regional rainfall and temperature change across India. Environ Res Commun 1:125002. https://doi.org/10.1088/2515-7620/ab4ee2

Zadeh LA (1999) Fuzzy sets as a basis for a theory of possibility. Fuzzy Sets Syst 100:9–34. https://doi.org/10.1016/S0165-0114(99)80004-9

Zhao T, Dai A (2017) Uncertainties in historical changes and future projections of drought. Part II: model-simulated historical and future drought changes. Clim Chang 144:535–548. https://doi.org/10.1007/s10584-016-1742-x